https://doi.org/10.1016/j.scs.2021.103007

An air curtain surrounding the solar tower receiver for effective reduction of convective heat loss

Qiliang Wang [1, *], Yao Yao [1], Mingke Hu [2], Jingyu Cao [3], Yu Qiu [4], Hongxing Yang [1, *]

[1] *Renewable Energy Research Group (RERG), Department of Building Services Engineering, The Hong Kong Polytechnic University, Hong Kong, China*

[2] *Institute of Sustainable Energy Technology, University of Nottingham, University Park, Nottingham NG7 2RD, UK*

[3] *Department of Thermal Science and Energy Engineering, University of Science and Technology of China, Hefei 230027, China*

[4] *School of Energy Science and Engineering, Central South University, Changsha, Hunan, 410083, China*

* Corresponding author.

E-mail address: hong-xing.yang@polyu.edu.hk (H. Yang); qiliang.wang@polyu.edu.hk (Q. Wang)

Abstract

External-type solar tower receiver, mounted on the top of a tower with an elevation of dozens or even hundreds of meters, is faced with unavoidably massive convective heat loss due to high operating temperature and high-speed wind at high altitude. To effectively reduce the convective heat loss, a novel solar tower receiver with an air curtain is proposed and designed. In this study, the comprehensive thermal performance of plant-scale tower receivers is numerically studied based on the finite volume method. The impacts of different configurations of air nozzles on the thermal

performance of the solar tower receiver are investigated. Furthermore, techno-economic analyses on the Solar Two power plant are also carried out. The results show that, in scenario of incoming wind speed of 15 m/s, the air curtain exerts the best roles at the air-jet angle of 45°, a distance of 1.50 m from the receiver surface, and air-jet velocity of 16 m/s in an operating mode of switching off the air nozzles at the windward and leeward sides. Compared with the original receiver, the heat loss of the proposed receiver is effectively reduced by 9.60 %, and the efficiency and electricity power production are enhanced by approximately 0.49 %.

Keywords: *Solar tower receiver; Concentrated solar power (CSP); Heat loss; Air curtain; Efficiency*

Nomenclature

c	Specific heat capacity, J/(kg·K)	μ_t	Turbulent viscosity, kg/m·s
D	Distance, m	ρ	Density, kg/m^3
g	Gravitational acceleration, m/s^2	φ	circumferential angle, °
I	Radiation intensity, W/m^2	***Abbreviation***	
k	Turbulence kinetic energy, m^2/s^3	a	Ambient
p	Pressure, Pa	AC	Air curtain
Q	Net heat flux, W/m	conv	convection
T	Temperature, °C	C	Column
u	Velocity, m/s	ETR	External-type tower receiver
v	Velocity, m/s	ETR-AC	ETR with an air curtain
Greek Symbols		CSP	Concentrated solar power
ε	Turbulence dissipation rate, m^2/s^3	HL	Heat loss
		HTF	Heat transfer fluid

η	Efficiency	P	Percentage
θ	Air-jet angle, °	R	Row

1. Introduction

Among all of the natural sources of energy, solar energy is being placed much great expectations in the new energy uses of the future because of its unique features of boundlessness and universal accessibility [1]. As one of dominant tehchnologies, solar thermal conversion has been demonstrated to be an efficient and sustainable solutions for providing heat for domestic [2] and industrial utilizations [3]. Concentrated solar thermal conversion is a burgeoning and increasing-known technology to harvest high-temperature heat energy for solar desalination [4], solar cooling [5], solar thermochemistry [6], concentrated solar power (CSP) [7], etc. Concentrated solar-thermal technology mainly includes four kinds of technical forms: solar tower collector [8], parabolic trough collector [9, 10], dish collector [11], and Fresnel collector [12]. The solar tower collector system is pretty promising for the utilization in the concentrated solar power (CSP) [13, 14], which is mainly composed of a solar tower receiver, large-scale heliostats, and two-axis tracking systems [15]. Heat transfer fluid (HTF) flows inside the solar tower receiver and is used to carry and transfer the thermal energy [16]. At present, the operating temperature of the tower receiver in a CSP plant could reach 560 °C when the HTF of the molten salt is employed [17]. In the future, the operating temperature would be further enhanced to even 700 °C for the solar tower receiver using supercritical carbon dioxide as the HTF [18, 19]. On account of receiving the concentrated sunrays reflected by the large-scale heliostats on the ground, the tower receiver needs to be mounted on the top of the tower, which has a height of dozens or even hundreds of meters [20]. Unlike the land surface, the cross-flow velocity at such a high

altitude is much higher, reaching above 10 m/s [21]. In conjunction with high operating temperatures, massive convective heat loss occurs in the external-type solar tower receiver, severely reducing the receiver efficiency and electric energy production of a CSP plant [22]. Therefore, it would be of significant value for the external-type receiver to effectively reduce the convective heat loss and enhance thermal performance.

For a long time, many researchers have carried out experimental and numerical investigations on the convective heat loss and thermal performance of external-type tower receivers [23, 24]. Kim et al. [25] numerically analyzed the convective and radiation heat loss of the external-type tower receiver without the cavity by CFD simulation. The results showed that, at the receiver temperature of 600 °C, the convective loss of the external-type tower receiver with a surface area of 9 m^2 significantly increased from 150.4 kW to 278.2 kW at the uniform cross-flow velocity varied from 5 m/s to 10 m/s. Pacheco et al. [13] carried out experiments on the Solar Two system [26] under different wind velocities. The experimental data demonstrated that the significantly increased convective heat loss of the external-type tower receiver at the wind velocity from 0.5 to 6.4 m/s resulted in a severe reduction by 2.4 % of receiver efficiency. The studies mentioned above prove the wind velocity at high altitudes exerts dramatic impacts on the thermal performance of an external-type tower receiver. However, little progress in the optimization methods for reducing the convective heat loss in the external-type tower receiver has been made.

Unlike the external-type tower receiver, the cavity-type tower receiver only has one flat aperture to pass through and receive the concentrated sunrays [27]. Based on the unique geometry of the cavity-type tower receiver, a method of installing an air nozzle on the top of the aperture was proposed by

Fang et al. [28] and Alipourtarzanagh et al. [29] to reduce the convective heat loss. The formed air curtain downward behaved like an “invisible wall”, which prevents the high-temperature air inside the cavity from flowing outside and thus reduces the natural convective heat loss. The results showed that the air curtain exerted effective roles in suppressing the natural convective inside the cavity. So far, however, no researchers have employed the air curtain method in the external-type tower receiver to reduce the convective heat loss. For the external-type tower receiver, conceivably, the air curtain may also be an effective way to block the oncoming cross-flow and reduce the turbulence near the receiver surface, thus reducing the convective heat loss.

Based on the explanation above, this study aims to validate the feasibility of the air curtain method in the external-type tower receiver (ETR) to reduce the convective loss. Unlike the cavity-type tower receiver, all receiver panel surfaces of the external-type tower receiver are exposed in the air to receive the concentrated sunrays from all around [30]. Thus the strong crosswind directly impinges on the external-type tower receiver surface, which would bring much more challenges to realize the effectiveness of the air curtain in the external-type tower receiver. In this work, the air curtain machines with air nozzles are proposed to circumferentially mount on the insulated box above the tower receiver for generating a high-velocity air curtain (AC) around the receiver. The proposed air curtain is expected to effectively prevent the high-velocity crosswind from sweeping the receiver surface and reduce the air turbulence near the receiver surface, thus lowering the convective heat loss. In this framework, the circumferential air curtain machines are uniformly split into eight parts, and each part has an air nozzle. A three-dimension model of the ETR with an air curtain (ETR-AC) is established. The thermal performance of ETR-AC is numerically studied for the optimum operating strategy of air nozzles.

Furthermore, the impacts of different configurations of the air nozzles, namely, air-jet angle, the distance between the air nozzles with the tower receiver, and air-jet velocity, on the thermal performance of the ETR-AC are investigated. Finally, the receiver efficiency and techno-economic analyses on the Solar Two power plant with the proposed ETR-AC are also investigated in this study.

2. Modelings of geometry and heat transfer

2.1 Geometry modeling of tower receiver

In this study, we employed the Solar Two plant (10 MWe) as the study object, which is located in Mojave Deserve [31]. The external-type tower receiver (ETR) in the Solar Two plant is mounted on the top of a tower with an elevation of 76 m. The radius and height of the cylindrical receiver in the ETR are 2.55 and 6.10 m, respectively [32]. The top and bottom parts of the receiver in the ETR are insulated boxes. The receiver surface is coated with black Pyromark paint, which has a solar radiation absorptivity of 0.9 and an emissivity of 0.88 [22].

The simplified schematic diagram of the proposed three-dimension ETR integrated with AC (ETR-AC) is exhibited in Fig. 1. Air curtain machines are placed above the receiver and surround the top insulated box, which could not block the receiver from receiving the incident concentrated solar radiation reflected from the heliostats. The circumferential air curtain machines are uniformly split into eight parts, and each part has one air nozzle corresponding to one inlet as shown in Fig. 1, i.e., *inlet 1*, *inlet 2*, …, *inlet 8* in sequence with the circumferential angle (φ) from 0 to 360° with an interval angle of 45°. The width of the inlet surface (air nozzle) is determined as 0.3 m. The angle of air-jet surfaces (namely, *inlets 1-8*) of the air nozzles toward the external air domain is set as θ. As shown in

Fig. 1, the angle of θ is defined as the angle between the normal of inlet surface ($\overrightarrow{PM}$) and vertical line ($\overrightarrow{PN}$). Furthermore, to accurately observe the thermal performance of the receiver surface at various positions, the receiver surface is evenly split into 4 sections (rows) from top to bottom and 8 sections (columns) in the circumferential. Therefore, total 32 equal zones are obtained as exhibited in Fig. 1. Each row's height is 1.55 m, and the circumferential angle occupied by each column is 45°, corresponding to an air nozzle. The detailed parameters of the ETR and ETR-AC are presented in Table 1.

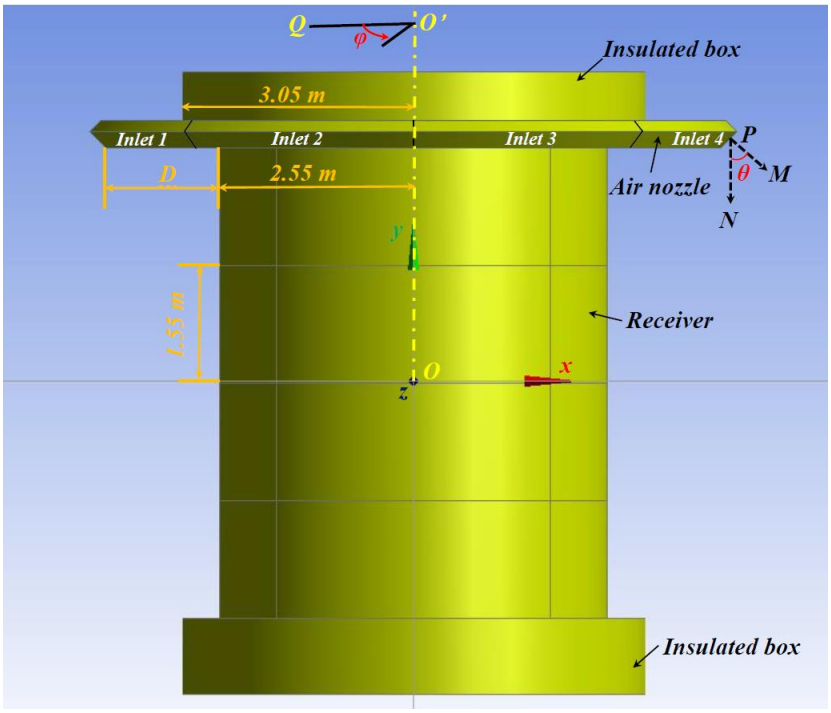

Fig. 1 Geometry of the proposed three-dimension external-type tower receiver with an air curtain (ETR-AC)

Table 1 Parameters of ETR and ETR-AC [22, 32]

Parameter	Value	Parameter	Value
Receiver elevation	76 m	Emissivity of coating	0.88
Receiver height	6.2 m	Inlet (1-8) width of nozzle	0.3 m

Receiver radius	2.55 m	Distance between nozzles and receiver (D)	1, 1.25, 1.5, 1.75, 2 m
Absorptivity of coating	0.9	air-jet angle (θ)	0, 30, 45, 60, 90°

2.2 Heat transfer modeling of tower receiver

In this study, a modeled external air domain was determined for numerical computation by Workbench in Ansys. As shown in Fig. 2, the dimensions of the external air domain are 40×40×60 m (length×width×height), which are much larger than those of ETR located in the center of the external air domain. The external wind comes by *inlet* surface, flows through the air domain along the x-axis, and leaves by *outlet* surface. Subsequently, around 550,000 tetrahedral grids of the external air domain were generated by Workbench mesh and used for the numerical calculations by CFD FLUENT (Fig. 3). The fine grids (for the receiver and air nozzles) to coarsen ones (for the external air domain) were used for fast calculation and desired accuracy. The average and maximum values of grid skewness were 0.51 and 0.92, respectively, which demonstrated the grid has good quality to accurately predict the performance of ETR and ETR-AC.

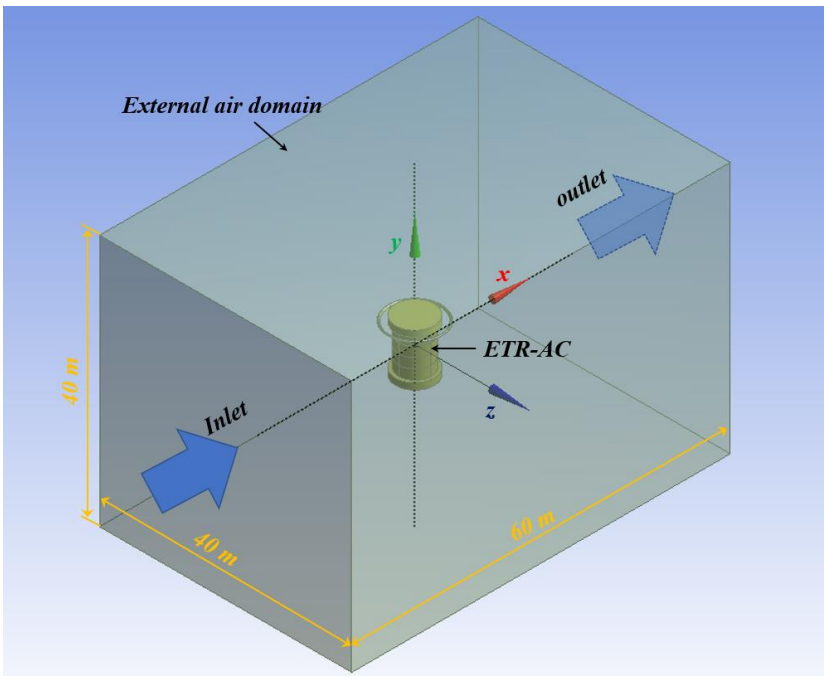

Fig. 2 Modeled external air domain and ETR-AC

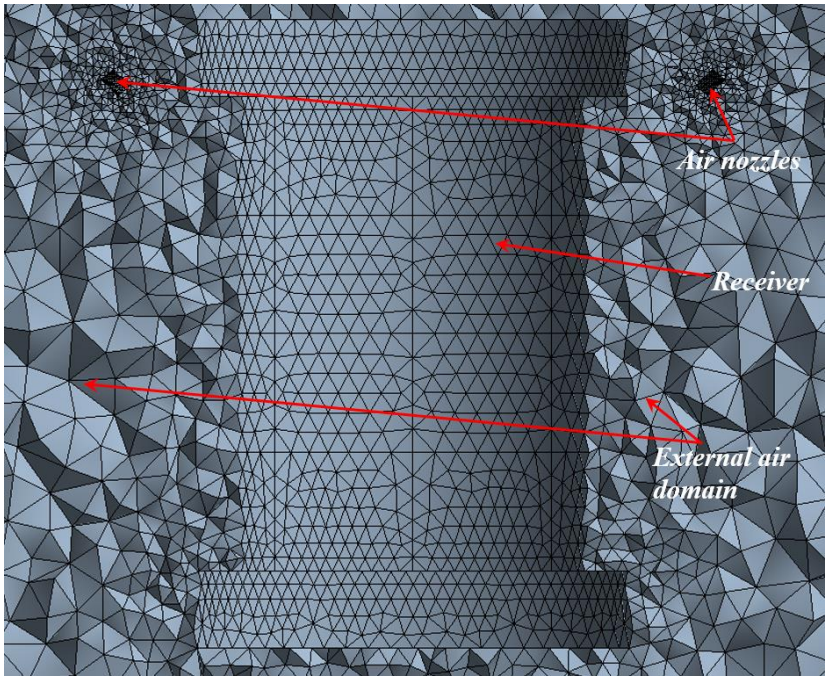

Fig. 3 Mesh of the model

The heat transfer processes under a steady state, including convective and radiative heat transfer from the receiver surface to the surroundings and sky, are stimulated by the finite volume method (FVM) in FLUENT 18.0 software. Standard *turbulence kinetic energy - turbulence dissipation rate* (*k-*

ε) turbulence model and discrete ordinates radiation model are employed in FlUENT software [33] to study the convective and radiative heat transfer. The detailed boundary conditions in the models of ETR and ETR-AC are listed in Table 2.

Table 2 Boundary conditions in the models of ETR and ETR-AC [22]

Item	Boundary	Value	Item	Boundary	Value
Inlet of external air domain	Velocity rate	10, 15, 20 m/s	Inlets of air nozzles	Velocity rate	5-15, 10-20, 15-25 m/s
Outlet of external air domain	Pressure outlet	0 Pa	All other surfaces except receiver surface	Adiabatic	\

The related equations involved in the models, namely, continuity equation, momentum equation, energy equation, *k and* ε equations, radiative equation, are presented as follows [22].

Continuity equation:

$$\frac{\partial(\rho u_j)}{\partial x_j} = 0 . \tag{1}$$

Momentum equation:

$$\frac{\partial(\rho u_i u_j)}{\partial x_j} = -\frac{\partial p}{\partial x_i} + \frac{\partial}{\partial x_j}[(\mu_t + \mu)(\frac{\partial u_i}{\partial x_j} + \frac{\partial u_j}{\partial x_i} - \frac{2}{3}\frac{\partial u_l}{\partial x_l}\sigma_{ij})] + \rho g_i , \tag{2}$$

where μ_t is the turbulent viscosity and can be calculated by:

$$\mu_t = \frac{C_\mu \rho k^2}{\varepsilon} . \tag{3}$$

Energy equation:

$$\frac{\partial(\rho u_j T)}{\partial x_j} = \frac{\partial}{\partial x_j}[(\frac{\mu}{\Pr} + \frac{\mu_t}{\sigma_t})\frac{\partial T}{\partial x_j}] + \frac{S_T}{c_p}. \quad (4)$$

Turbulence kinetic energy (k) equation:

$$\frac{\partial(\rho u_j k)}{\partial x_j} = \frac{\partial}{\partial x_j}[(\mu + \frac{\mu_t}{\sigma_k})\frac{\partial k}{\partial x_j}] + \mu_t \frac{\partial u_i}{\partial x_j}(\frac{\partial u_i}{\partial x_j} + \frac{\partial u_j}{\partial x_i}) - \rho\varepsilon. \quad (5)$$

Turbulence dissipation rate (ε) equation:

$$\frac{\partial(\rho u_k \varepsilon)}{\partial x_k} = \frac{\partial}{\partial x_k}[(\mu + \frac{\mu_t}{\sigma_\varepsilon})\frac{\partial \varepsilon}{\partial x_k}] + C_1 \frac{\varepsilon}{k}\mu_t \frac{\partial u_i}{\partial x_j}(\frac{\partial u_i}{\partial x_j} + \frac{\partial u_j}{\partial x_i}) - C_2 \rho \frac{\varepsilon^2}{k}. \quad (6)$$

In Equations (3), (5) and (6), the parameters of C_μ, σ_k, σ_ε, C_1, and C_2 are constants, i.e., 0.09, 1.0, 1.3, 1.44, and 1.92, respectively.

Radiative equation:

$$\nabla(I_r(\vec{r},\vec{d})\vec{d}) = 0, \quad (7)$$

where I_r represents the radiation intensity; $\vec{r}$ and $\vec{d}$ refer to the position vector and direction vector in the air, respectively.

As a result, the solar receiver efficiency (η) can be expressed as follows:

$$\eta = \frac{Q_{abs}}{Q_{abs} + Q_{loss}}, \quad (8)$$

where Q_{abs} and Q_{loss} refer to the absorbed power by the receiver and total heat loss of the receiver (W). The total heat loss includes the convective and radiative heat loss from the receiver loss.

3. Model validation

3.1 Grid independence check

Grid number exerts an important impact on the simulated results in the case of inadequate meshing used for calculations. To ensure good meshing and eliminate the effect of grid numbers on the results, grid independence checks have been carried out in this section. Assuming that the external incoming wind velocity, ambient temperature, and receiver temperature are 5 m/s, 23 ℃, and 530 ℃, the simulated results of convective heat loss of ETR generated with five different grid numbers (around 27000, 66000, 210000, 550000, and 900000) are exhibited in Fig. 4. It is observed that the convective heat loss of ETR significantly increases with the increasing grid number from 27000 to 550000, but has no apparent changes at the grid number exceeding 550000; which demonstrates the simulated results almost eliminate the dependence on the grid number when the grid number is equal to and larger than 550000 in this study. Therefore, the grid number of 550000 is adopted in this work to conduct accurate and fast calculations.

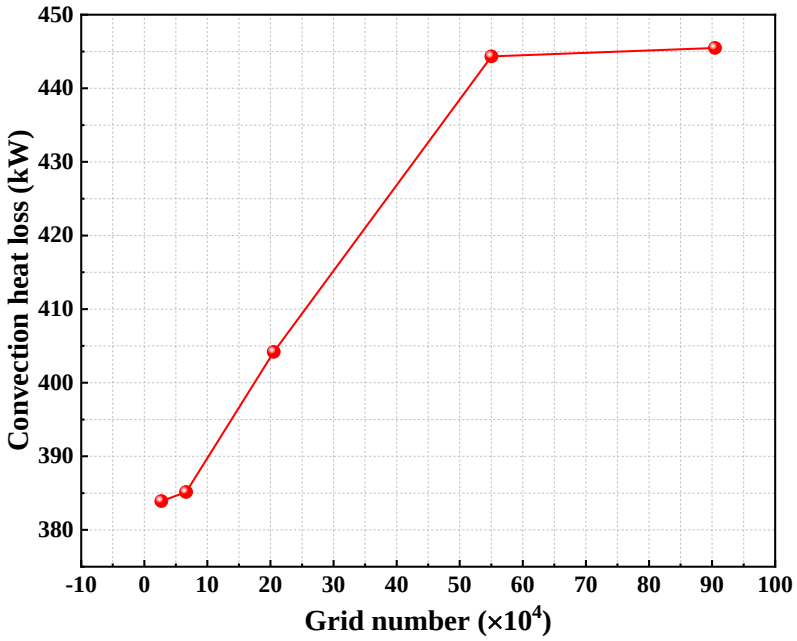

Fig. 4 Convective heat loss of ETR under different grid numbers

3.2 Validation of heat transfer model

To validate the model used in this study, the calculated receiver efficiencies are compared with actual experimental data conducted by Sandia National Laboratories [23] and simulation data carried out by Kim et al. [25]. The simulated receiver efficiencies under the same experimental conditions are exhibited in Table 3. At different incoming wind velocities from 0.5 to 6.4 m/s, the calculation errors of receiver efficiency in literature [25] and this study maintain within ± 2.0 and 1.5 %, respectively, demonstrating that the simulated results in this study yield good consistencies with the experimental data and have better accuracies than the simulated results in [25]. Therefore, it is proved that the models developed in this study can accurately predict the performance of ETR and ETR-AC.

Table 3 Comparisons of calculated receiver efficiency with the experimental and other simulated data

Wind velocity (m/s)	Power absorbed (MW)	Receiver efficiency			Errors in [25] (%)	Errors in this study (%)
		Measured data	Calculated results in [25]	Calculated results in this study		
0.5	34.3	0.880	0.885	0.879	-0.57	-0.11
0.8	27.7	0.870	0.885	0.863	1.72	-0.80
1.2	31.5	0.874	0.878	0.871	0.46	-0.34
1.5	27.7	0.881	0.867	0.870	-1.59	-1.25
2.5	31.5	0.866	0.875	0.868	1.04	0.23
6.4	25.0	0.856	0.843	0.848	-1.52	-0.93

4. Results and discussions

4.1 Operating modes of air nozzles

As explained above, the circumferential air nozzles around the receiver are split into eight parts, i.e., air nozzles 1-8. To achieve the optimum performance of the ETR-AC, three kinds of operating modes of air nozzles in the ETR-AC are performed. In this section, the external incoming wind velocity, ambient temperature, and receiver temperature are determined as 15 m/s, 23 ℃, and 600 ℃.

The convective heat loss of the receiver surface at different zones in the original ETR without air nozzles is exhibited in Fig. 5. For the sake of simplicity, each one of total 32 zones is symbolized by a combination of row and column. For example, the zone located in the first row (*R1*) and first column (*C1*) is symbolized as *R1-C1*; similarly, the zone located in the fourth row (*R4*) and eighth column (*C8*) is symbolized as *R4-C8*. It is observed from Fig. 5 that convective heat losses in *column 1* and *column 8* of the receiver surface are minimal compared with other columns. That is because, when the external incoming wind transversely flows around the cylindrical ETR, stagnation behavior occurs at the front of the receiver surface (i.e., front of *column 1* and *column 8*); subsequently, a boundary layer will be formed on the receiver surface. The stagnation behavior and boundary layer would result in a significant decrease in wind velocity, thus reducing the receiver surface's convective heat transfer coefficient at *column 1* and *column 8*. With further development of the boundary layer, wind velocity along the receiver surface is gradually enhanced, thus leading to higher convective heat loss in *columns 2*, *3*, *6*, and *7*. The receiver surface at *columns 4* and *5*, which is the downstream area of wind around the receiver, emits the largest convective heat loss due to separation of the boundary layer and incurred great airflow turbulence.

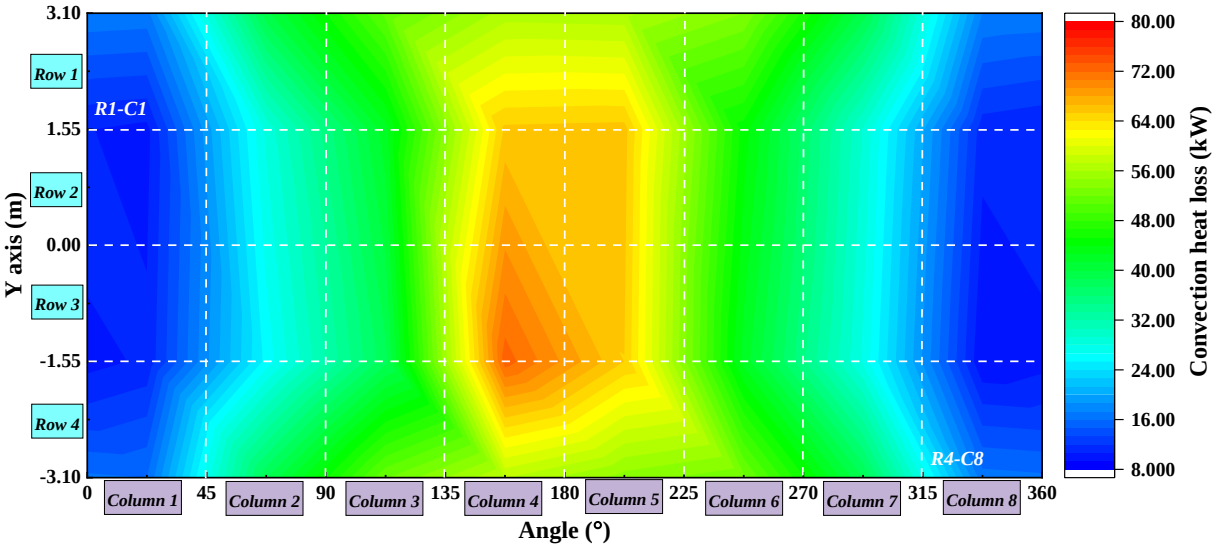

Fig. 5 Contour of convective heat loss of receiver surface in original ETR

To obtain the optimum performance of ETR, three kinds of ETR-ACs with different air nozzles switched on, namely, ETR-AC with all nozzles 1-8 switched on (Type A), ETR-AC with nozzles 2-7 switched on (Type B), and ETR-AC with nozzles 2/3/6/7 switched on (Type C), are investigated in this section. It needs to be emphasized that the air-jet velocity and air-jet angle of air nozzles, and the distance between air nozzles and receiver surface in three kinds of ETR-ACs are determined as 16 m/s, 45°, and 1.5 m in this section, respectively.

Contours of convective heat loss of receiver surface at different zones in three kinds of ETR-ACs are exhibited in Fig. 6. Compared with the original ETR, the convective heat loss of receiver surface at *columns 4* and *5* in type-A ETR-AC is visually reduced as shown in Fig. 6 (a), i.e., *R1-C4*, *R2-C4*, *R3-C4*, *R4-C4*, *R1-C5*, *R2-C5*, *R3-C5*, and *R4-C5*. The total convective heat losses of the receiver surface at *columns 4* and *5* in the ETR and type-A ETR-AC are 252.4 and 241.6 kW, 244.2 and 234.2 kW, respectively; it is calculated that the total convective heat losses of the latter are reduced by approximately 3.3 and 3.1 % for the *columns 4* and *5* compared with those of the former, respectively.

The reason for this phenomenon is that the high-speed air curtain formed due to the nozzles cuts off part of the external incoming wind; thus, less airflow turbulence occurs at *columns 4* and *5*. However, the convective heat loss of the receiver surface in type-A ETR-AC at *columns 1* and *8* increases in contrast to the original ETR, especially those at zones of *R1-C1* and *R1-C8*. The convective heat losses of the receiver surface at zones of *R1-C1* and *R1-C8* in the original ETR and type-A ETR-AC are 16.8 and 17.3 kW, 20.1 and 21.3 kW, respectively. The convective heat losses of the latter are increased by 20.1 and 23.1 % for the zones of *R1-C1* and *R1-C8* compared with those of the former. The reason for this phenomenon is that the high-speed jetted air for *nozzles 1* and *8* breaks the stagnation behavior and boundary layer and results in local turbulence, and the convective heat coefficients at the front of the receiver surface (i.e., zones of *R1-C1 and R1-C8*) are correspondingly increased.

To eliminate the negative effects incurred by the jetted air from *nozzles 1* and *8*, a type-B ETR-AC which shuts off *nozzles 1* and *8* is proposed. As shown in Fig. 6 (b), the convective heat losses of type-B ETR-AC at zones of *R1-C1* and *R1-C8* are reduced to 16.2 and 16.0 kW with percentage-reduction roughly about 24.1 and 24.9 % compared with type-A ETR-AC. Therefore, it is proved to contribute to ensuring the boundary layer's integrity and thus reducing the convective heat loss at the front of the receiver surface when *nozzles 1* and *8* are shut off. Nevertheless, it is noticed that the convective heat losses of the receiver surface at *columns 4* and *5* are still excessive and thus lead to a difficulty of further significant reduction of convective heat loss. Considering a probability of limited role of *nozzles 4* and *5* in reducing the convective heat loss of the receiver surface at *columns 4* and *5*, subsequently, a type-C ETR-AC with nozzles 2/3/6/7 switched on is put forward to verify the effect of this new operation mode of air nozzles on the thermal performance of the receiver. As exhibited in Fig.

6 (c), the convective heat losses of the receiver surface at *columns 4* and *5* are greatly reduced compared with the type-B ETR-AC, which proves that the shutdowns of *nozzles 4* and *5* do exert positive impacts on the reduction of convective heat loss at *columns 4* and *5*. This is because *columns 4* and *5* are located in the downstream area of external incoming wind around the receiver, the jetted air from *nozzles 4* and *5* is hard to effectively block the external wind like the lateral *nozzles 2/3/6/7*, but would strengthen the turbulence of wake, thus leading to additional convective heat loss at *columns 4* and *5*.

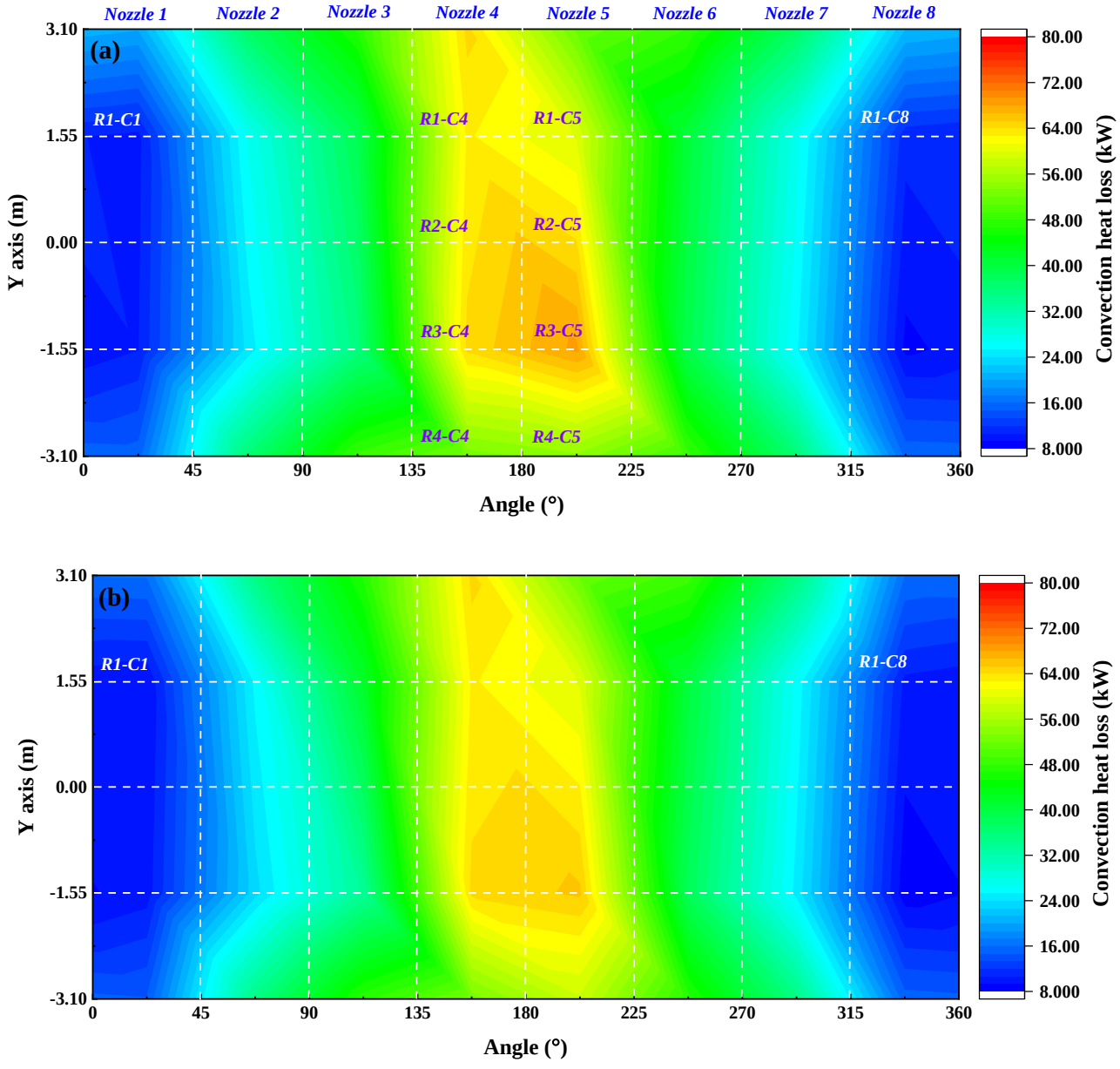

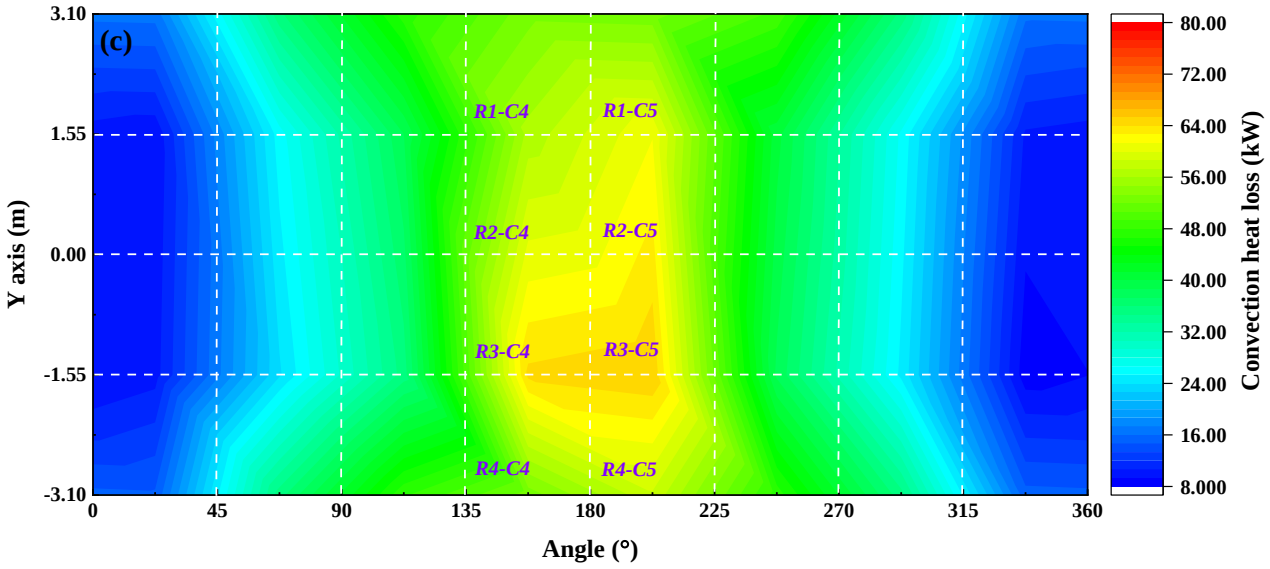

Fig. 6 Contours of convective heat loss of receiver surfaces in (a) ETR-AC with all nozzles 1-8 switched on (Type A), (b) ETR-AC with nozzles 2-7 switched on (Type B), and (c) ETR-AC with nozzles 2/3/6/7 switched on (Type C).

In conclusion, the original ETR and three types of ETR-AC with different operation modes of air nozzles are proposed, investigated, and compared in this section. The complete results of convective heat loss and receiver efficiency are exhibited in Fig. 7(a) and (b). As analyzed above, it is observed that the type-C ETR-AC harvests the best thermal performance compared with the original ETR, type-B and type-A ETR-AC are inferior to type-C ETR-AC in order. The total convective heat losses and receiver efficiencies of the original ETR and type-C ETR-AC are 1.246 and 1.131 MW, 0.814 and 0.818, respectively. Accordingly, reduction of convective heat loss and enhancement of receiver efficiency in % of type-C ETR-AC are calculated as 9.23 and 0.49 compared with the original ETR, respectively. Therefore, the method of air curtain surrounding the ETR is proved an effective way to reduce the convective heat loss and enhance the receiver efficiency.

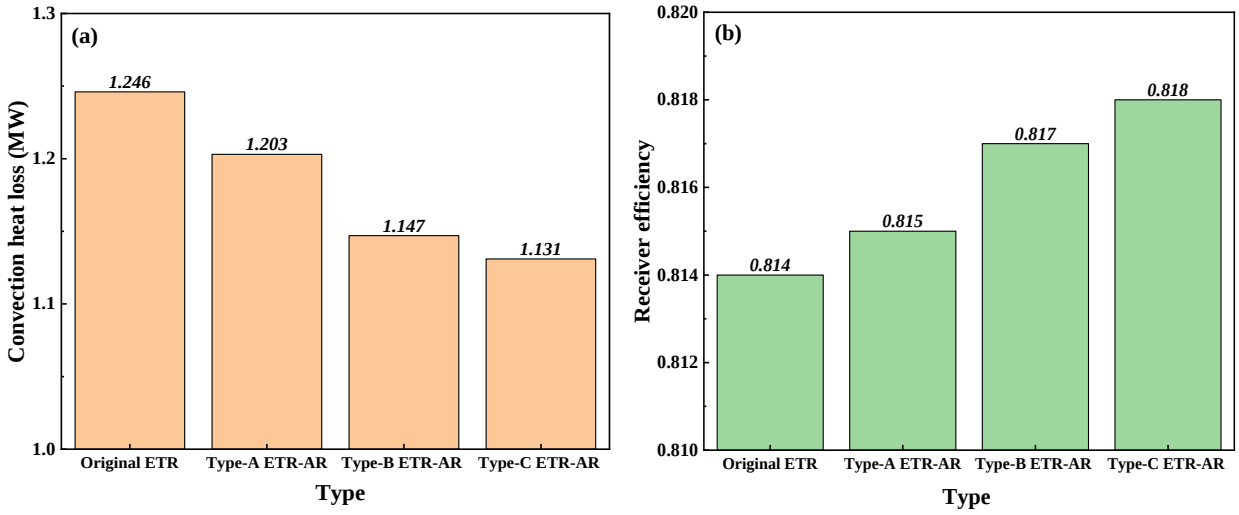

Fig. 7 Convective heat loss and receiver efficiency of four kinds of ETRs

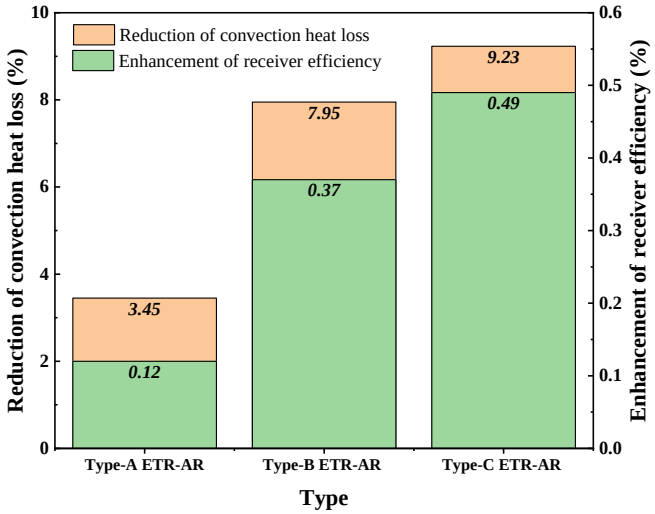

Fig. 8 Reduction of convective heat loss and enhancement of receiver efficiency in % of ETR-ACs with different operation modes of air nozzles

4.2 Parametric analyses on air nozzles

The effectiveness of the air curtain on the receiver is greatly related to the key parameters of the configuration of air nozzles, namely, air-jet angle (i.e., θ as exhibited in Fig. 1), distance between the nozzles and receiver surface ((i.e., D as exhibited in Fig. 1)), and air-jet velocity. In this section, under the determined external incoming wind velocity of 15 m/s, ambient temperature of 23 ℃, and receiver temperature of 600 ℃, the impacts of different dimensions of these parameters on the thermal

performance of the type-C ETR-AC are studied for achieving the optimum configurations of ETR-AC.

Firstly, the impacts of different air-jet angles varied from 0 to 90° are investigated in the case where the distance (D) and air-jet velocity are set as 1.5 m and 16 m/s, respectively. The simulated results are presented in Fig. 9. When the value of air-jet angle is set as 0 or 90°, indistinctive change of convective heat loss from the receiver surface in type-C ETR-AC appears compared with the original ETR; which demonstrates that the air curtain with too small or too large air-jet angle exerts limited roles in blocking the external incoming wind and reducing the convective heat loss. In contrast, relatively better thermal performance is obtained for the ETR-AC with the air-jet angle ranging from 30 to 60°, of which the ETR-AC with an air-jet angle of 45° achieves the best thermal performance with the lowest convective heat loss of 1.131 MW, approximately 9.23 % reduction compared with the original ETR. Therefore, it can be concluded that a proper air-jet angle should be around 45° for obtaining the best blockage effect on the incoming crosswind.

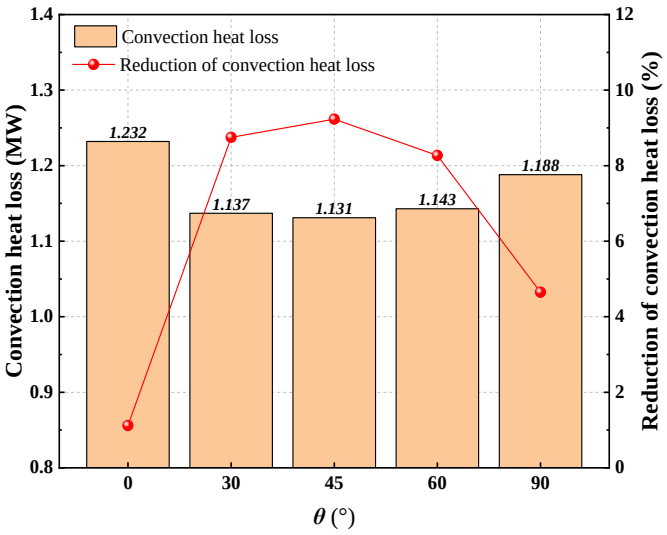

Fig. 9 Convective heat loss and reduction of convective heat loss in percentage of ETR-ACs with different air-jet angles

The distance between air nozzles and receiver surface also impacts the thermal performance of the ETR-AC. The computations are carried out under the fixed values of air-jet angle of 45° and air-jet velocity of 16 m/s. As shown in Fig. 9, there has a certain effect on reducing the convective heat loss of ETR-AC when a short distance (1.00 or 1.25 m) is determined for the air nozzles, approximately 6.0 % heat loss reduction compared with the original ETR. ETR-AC possesses the best thermal performance in the case of a distance of 1.50-1.75 m, in which the convective heat losses are reduced to 1.131-1.135 MW and the corresponding reduction percentages reach 9.23-8.91%. On the contrary, the worst thermal performance of ETR-AC occurs at a distance of 2.00 m, the convective heat loss of ETR-AC is reduced by only 2.97 % compared with the original ETR. The results above demonstrate that the nozzles with a distance below 1.50 m would cause airflow disturbance near the receiver surface and exert a negative influence on the reduction of convective heat loss; besides, the nozzles with a distance above 1.75 m also play limited roles in the blockage of incoming wind and the reduction of convective heat loss due to too far away from the receiver surface. Therefore, 1.50-1.75 m is a suitable range of distance for the air nozzles to achieve the best thermal performance.

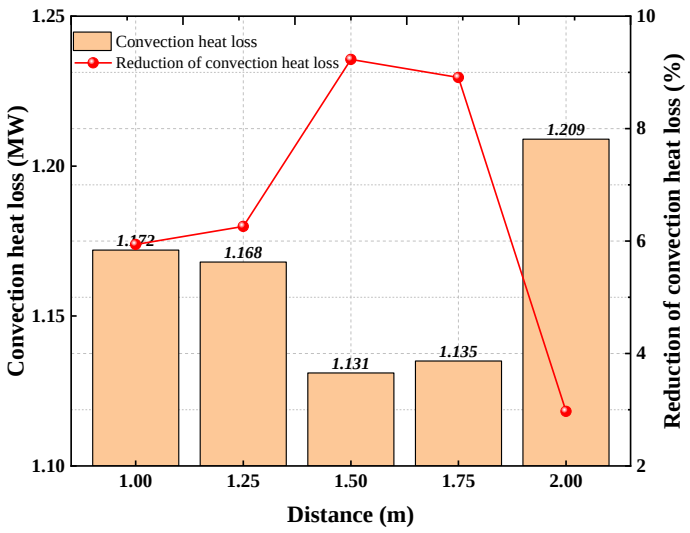

Fig. 10 Convective heat loss and reduction of convective heat loss in percentage of ETR-ACs with different distances

Without a doubt, air-jet velocity is another key parameter for the ETR-AC to achieve the optimum thermal performance. The other two parameters, i.e., air-jet angle and distance (*D*) and, are set as 45° and 1.5 m, respectively. The calculated results are presented in Fig. 11. It can be observed that the air curtain generated by nozzles in the ETR-AC works at its best when the air-jet velocity ranges from 14 to 16 m/s, the corresponding convective heat losses are reduced by approximately 8.99 and 9.23 %, respectively. In contrast, the air curtain with lower and higher air-jet velocities could not exert the best roles in reducing the convective heat loss. Those are because the air curtain with lower air-jet velocity cannot effectively withstand the external incoming wind with higher speed, but the air curtain with higher air-jet velocity would increase turbulence at the local receiver surface. In conclusion, 14-16 m/s is a suitable range of air-jet velocity for the air nozzles to achieve the best thermal performance at an incoming wind speed of 15 m/s.

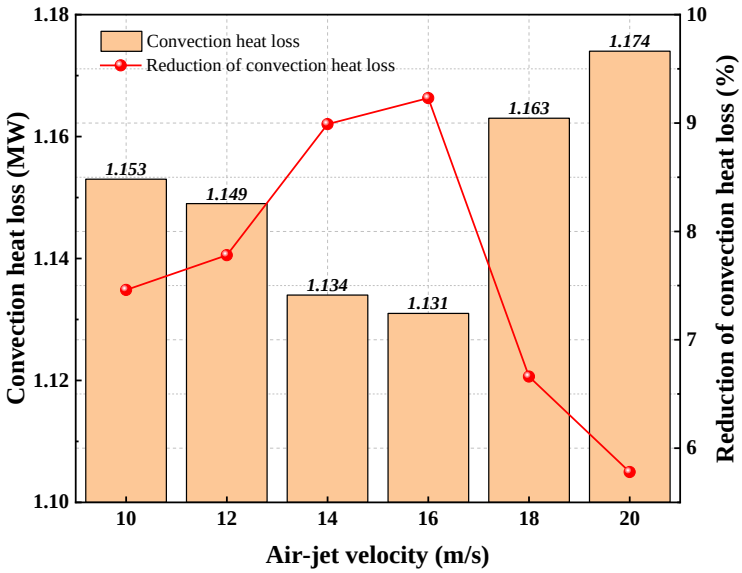

Fig. 11 Convective heat loss and reduction of convective heat loss in percentage of ETR-ACs with different air-jet velocities

Furthermore, the optimum air-jet velocities under different incoming wind speeds are calculated. As presented in Table 4, the optimum air-jet velocities are close to the external incoming wind speeds; when the external incoming wind speeds are 10, 15, and 20 m/s, the corresponding optimum air-jet velocities are 8, 16, and 18 m/s. Assuming the receiver temperature (T_r) and absorbed power by the receiver (Q_{abs}) are 600 °C and 30 MW, the convective heat loss and receiver efficiency in original ETR and ETR-AC are computed. It is observed that ETR-AC achieves superior performance compared with the original ETR under different external incoming wind speeds from 10 to 20 m/s. The maximum reduction of total heat loss in % ($P_{reduced}$) of ETR-AC compared with original ETR occurs at the low incoming wind speed of 10 m/s, reaching 9.89 %. With increasing incoming wind speed, the value of $P_{reduced}$ decreases slightly, but the enhancement of receiver efficiency in % ($P_{enhanced}$) increases. At the external incoming wind speeds of 10, 15, and 20 m/s, the values of $P_{enhanced}$ are 0.36, 0.49, and 0.62, respectively. It is thus concluded that the proposed air curtain will exert a better role in enhancing the receiver efficiency at higher external incoming wind speed.

Table 4 Optimum air-jet velocities corresponding to different incoming wind speeds and performance comparisons between the original ETR and proposed ETR-AC

v_{wind} (m/s)	T_r (°C)	Q_{abs} (MW)	Optimum $v_{air-jet}$ (m/s)	HL_{rad} (MW)	$HL_{conv,ETR}$ (MW)	$HL_{conv,ETR-AC}$ (MW)	$P_{reduced}$ (%)	η_{ETR}	η_{ETR-AC}	$P_{enhanced}$ (%)
10	600	30	8	2.84	0.91	0.82	9.89	0.825	0.828	0.36
15			16		1.25	1.13	9.60	0.814	0.818	0.49
20			18		1.55	1.41	9.03	0.803	0.808	0.62

4.3 Techno-economic analyses on Solar Two plants with the proposed tower receiver

To further validate the feasibility of the proposed ETR-AC, the techno-economic analyses on Solar Two plants with the original ETR and type-C ETR-AC are carried out. In this section, the receiver temperature, external incoming wind speed, and ambient temperature are set as 600 ℃, 15 m/s, and 23 ℃, respectively. As the same assumption above, the absorbed power of the receiver in Solar Two plant 30 MWt, and the calculated receiver efficiencies of the original ETR and ETR-AC are 0.814 and 0.818, respectively. According to the literature [21], the heat transfer/exchange efficiency and turbine efficiency of power are approximately 80 and 24 %. Therefore, the electricity powers of CSP plants with the original ETR and ETR-AC can be calculated as 664220 and 667490 kWe.

Due to the addition of air curtain machines in the ETR-AC, the air curtain machines' initial investment cost and electricity consumption should be considered in comprehensive analyses and comparisons. In this section, the optimum configurations of air curtain machines obtained above, namely, the air-jet angle of 45 °, the air-jet velocity of 16 m/s, and the distance of 1.5 m, are applied in the studied example. Besides, the air curtain machine (series: AFM3009-01) made by Airmate is employed [35]. The length of the machine is about 1525 mm, thus 16 machines are needed for meeting the demand of the ETR-AC. The total initial investment costs of machines include the purchasing expenses of machines and related corollary equipment around 4000 USD [35], installation and labor costs estimated around 8000 USD according to the average cost of the engineer in the USA (50 USD per hour per person) [36]. Thus the total initial investment is about 12000 USD, an extremely low value compared to the billions of dollars invested in a CSP plant [37]. Therefore, those additional investment costs of machines can be ignored. Considering the electricity consumption of a single

machine of about 640 We, the actual net electricity power of CSP installing ETR-AC is 667484 kWe, which is enhanced by approximately 0.49 % compared with that of the original ETR. That means the net annual electricity output of CSP with ETR-AC will be improved by 0.49 %. Therefore, the proposed ETR-AC will be of great economic value for the CSP plant.

Table 5 Metrics in Solar Two plants with the original ETR and ETR-AC (10 MWe)

Metric/Item	Original ETR	ETR-AC
Absorbed power	30 MWt	
Receiver temperature	600 °C	
Receiver efficiency	0.814	0.818
Heat transfer/exchange efficiency	80 %	
Turbine efficiency of power [34]	34 %	
Electricity power of CSP	664,220 kWe	667,490 kWe
Length of single air curtain machine [34]	\	1525 mm
Number of air nozzles (air curtain machines)	\	16
Total initial investment cost of air curtain machines [35, 36]	\	12,000 USD
Power of single air curtain machine	\	640 We
Net Electricity power of CSP	664,220 kWe	667,484 kWe

5. Conclusions

To effectively reduce the massive convective heat loss from the external-type tower receiver (ETR) incurred by the large external incoming wind, the study proposes and designs a novel ETR with an air

curtain (ETR-AC) surrounding the receiver. In this work, a three-dimension model based on the finite volume method is established and validated. The model is then employed to optimize the detailed configurations of ETR-AC, including the operation modes of the air nozzles (type-A, type-B, and type-C ETR-AC), air-jet angle, the distance between the air nozzles and receiver surface, and air-jet velocity, for achieving optimal operating strategy of the air nozzles and thus the best thermal performance of ETR-AC. Furthermore, the thermal efficiency and techno-economic analyses of the Solar Two power plant with ETR-AC are also investigated. The main conclusions of this work are summarized as follows:

(1) With a grid number not lower than 550000, the simulated results of convective heat loss from the ETR basically eliminate the dependence on the grid number. And the calculation errors of receiver efficiency by the model maintain ± 1 % compared with the experimental data. These demonstrate that the model with a grid number of 550000 can accurately carry out the computations of heat loss, receiver efficiency.

(2) The air curtain surrounding the ETR is an effective method to reduce the convective heat loss and enhance the receiver efficiency. Among three types of ETR-ACs, the type-C ETR-AC, with an operating mode by switching on the nozzles 2/3/6/7 but off the nozzles 1/4/5/8, achieves the best thermal performance. Compared with the original ETR, reduction of convective heat loss and enhancement of receiver efficiency in % of type-C ETR-AC are calculated as 9.23 and 0.49, respectively.

(3) To obtain the best blockage effect on the incoming crosswind and thus reducing the convective heat loss, the optimum configurations of the ETR-AC are concluded at an external incoming wind speed of 15 m/s, i.e., air-jet angle of around 45°, distance range of 1.50-1.75 m, and air-jet velocity range of 14-16 m/s. The total heat loss and receiver efficiency of ETR-AC with the optimum configurations are reduced by 9.60 % from 1.25 MW in the original ETR to 1.13 MW, and enhanced by 0.49 % from 0.814 in the original ETR to 0.818, respectively.

(4) Considering the electricity consumption of air curtain machines, the actual net electricity power of CSP installing ETR-AC is enhanced by approximately 0.49 % compared with that of the original ETR. Therefore, the proposed ETR-AC will be of great economic value for the CSP plant.

Acknowledgment

This study was sponsored by the RGC Postdoctoral Fellowship Scheme 2020/2021 (3-RA59), the Postdoctoral Hub program (PiH/160/19) of the Innovation and Technology Fund of the Hong Kong SAR Government, and China Postdoctoral Science Foundation (2019M652209).

References

[1] Pitz-Paal R. Concentrating solar power: still small but learning fast. Nature Energy. 2017, 12;2(7):1-2.

[2] Zhou J, Zhao X, Yuan Y, et al. Operational performance of a novel heat pump coupled with mini-channel PV/T and thermal panel in low solar radiation[J]. Energy and Built Environment, 2020, 1(1): 50-59.

[3] Qin J, Hu E, Li X. Solar aided power generation: A review[J]. Energy and Built Environment, 2020, 1(1): 11-26.

[4] Wu G, Zheng H, Ma X, et al. Experimental investigation of a multi-stage humidification-dehumidification desalination system heated directly by a cylindrical Fresnel lens solar concentrator[J]. Energy Conversion and Management, 2017, 143: 241-251.

[5] Allouhi A, Kousksou T, Jamil A, et al. Solar driven cooling systems: An updated review[J]. Renewable and Sustainable Energy Reviews, 2015, 44: 159-181.

[6] Li W, Hao Y. Efficient solar power generation combining photovoltaics and mid-/low-temperature methanol thermochemistry[J]. Applied Energy, 2017, 202: 377-385.
[7] He Y L, Qiu Y, Wang K, Yuan F, Wang W Q, Li M J, Guo J Q. Perspective of concentrating solar power[J]. Energy, 2020, 198: 117373.
[8] Qiu Y, Li M J, Li M J, et al. Numerical and experimental study on heat transfer and flow features of representative molten salts for energy applications in turbulent tube flow[J]. International Journal of Heat and Mass Transfer, 2019, 135: 732-745.
[9] Wang Q, Yang H, Zhong S, et al. Comprehensive experimental testing and analysis on parabolic trough solar receiver integrated with radiation shield[J]. Applied Energy, 2020, 268: 115004.
[10] Wang Q, Shen B, Huang J, et al. A spectral self-regulating parabolic trough solar receiver integrated with vanadium dioxide-based thermochromic coating[J]. Applied Energy, 285: 116453.
[11] Pavlovic S, Loni R, Bellos E, et al. Comparative study of spiral and conical cavity receivers for a solar dish collector[J]. Energy Conversion and Management, 2018, 178: 111-122.
[12] Cheng Z D, Zhao X R, He Y L, et al. A novel optical optimization model for linear Fresnel reflector concentrators[J]. Renewable energy, 2018, 129: 486-499.
[13] Fernández A G, Gomez-Vidal J, Oró E, et al. Mainstreaming commercial CSP systems: A technology review. Renewable Energy 2019; 140: 152-176.
[14] Islam M T, Huda N, Abdullah A B, et al. A comprehensive review of state-of-the-art concentrating solar power (CSP) technologies: Current status and research trends[J]. Renewable and Sustainable Energy Reviews, 2018, 91: 987-1018.
[15] González-Roubaud E, Pérez-Osorio D, Prieto C. Review of commercial thermal energy storage in concentrated solar power plants: Steam vs. molten salts. Renewable and sustainable energy reviews 2017; 80: 133-148.
[16] Vant-Hull L L. Central tower concentrating solar power (CSP) systems[M]//Concentrating solar power technology. Woodhead Publishing, 2012: 240-283.
[17] Behar O, Khellaf A, Mohammedi K. A review of studies on central receiver solar thermal power plants[J]. Renewable and sustainable energy reviews, 2013, 23: 12-39.
[18] Wang K, Li M J, Zhang Z D, et al. Evaluation of alternative eutectic salt as heat transfer fluid for solar power tower coupling a supercritical CO2 Brayton cycle from the viewpoint of system-level analysis[J]. Journal of Cleaner Production, 2021, 279: 123472.
[19] Wang K, Zhang Z D, Li M J, et al. A coupled optical-thermal-fluid-mechanical analysis of parabolic trough solar receivers using supercritical CO2 as heat transfer fluid[J]. Applied Thermal Engineering, 2020, 183: 116154.
[20] Christian J M, Ho C K. CFD simulation and heat loss analysis of the solar two power tower receiver[C]//Energy Sustainability. American Society of Mechanical Engineers, 2012, 44816: 227-235.
[21] Hu T, Jia P, Wang Y, et al. Numerical simulation on convective thermal loss of a cavity receiver in a solar tower power plant[J]. Solar Energy, 2017, 150: 202-211.
[22] Wang W Q, Qiu Y, Li M J, et al. Coupled optical and thermal performance of a fin-like molten salt receiver for the next-generation solar power tower[J]. Applied Energy, 2020, 272: 115079.

[23] Pacheco J E, Bradshaw R W, Dawson D B, et al. Final test and evaluation results from the solar two project[J]. SAND2002-0120, 2002.
[24] Ballestrín J, Casanova M, Monterreal R, et al. Simplifying the measurement of high solar irradiance on receivers. Application to solar tower plants[J]. Renewable Energy, 2019, 138: 551-561.
[25] Kim J, Kim J S, Stein W. Simplified heat loss model for central tower solar receiver[J]. Solar Energy, 2015, 116: 314-322.
[26] H.E. Reilly, G.J. Kolb, An evaluation of molten-salt power towers including results of the Solar Two project. SAND2001-3674.
[27] Yan, Jian, You-duo Peng, and Zi-ran Cheng. Optimization of a discrete dish concentrator for uniform flux distribution on the cavity receiver of solar concentrator system[J]. Renewable energy 129 (2018): 431-445.
[28] Fang J, Tu N, Torres J F, et al. Numerical investigation of the natural convective heat loss of a solar central cavity receiver with air curtain[J]. Applied Thermal Engineering, 2019, 152: 147-159.
[29] Alipourtarzanagh E, Chinnici A, Nathan G J, et al. Experimental insights into the mechanism of heat losses from a cylindrical solar cavity receiver equipped with an air curtain[J]. Solar Energy, 2020, 201: 314-322.
[30] López-Herraiz M, Fernández A B, Martinez N, et al. Effect of the optical properties of the coating of a concentrated solar power central receiver on its thermal efficiency[J]. Solar Energy Materials and Solar Cells, 2017, 159: 66-72.
[31] Wang Q, Pei G, Yang H. Techno-economic assessment of performance-enhanced parabolic trough receiver in concentrated solar power plants[J]. Renewable Energy, 2020. 167: 629-643.
[32] Yang H, Li J, Wang Q, et al. Performance investigation of solar tower system using cascade supercritical carbon dioxide Brayton-steam Rankine cycle[J]. Energy Conversion and Management, 2020, 225: 113430.
[33] Gu Y, Pei J, Yuan S, et al. A Pressure Model for Open Rotor–Stator Cavities: An Application to an Adjustable-Speed Centrifugal Pump With Experimental Validation[J]. Journal of Fluids Engineering, 2020, 142(10).
[34] Schöttl P, Nitz P, Fluri T, et al. Simulation and optimization of solar tower plant receivers[J]. 12th SOLLAB Doctoral Colloqium, Rodalquilar, Almería, Spain, June 6-8, 2016: Book of Abstracts, 2016: 35-35.
[35] https://www.airmate.com/.
[36] https://www.dol.gov/general/topic/statistics/business.
[37] Malagueta D, Szklo A, Soria R, et al. Potential and impacts of Concentrated Solar Power (CSP) integration in the Brazilian electric power system[J]. Renewable Energy, 2014, 68: 223-235.